STEM CELLS

CANCER STEM CELLS

# Reprogramming Antagonizes the Oncogenicity of HOXA13-Long Noncoding RNA HOTTIP Axis in Gastric Cancer Cells

DENG-CHYANG WU,[a,b,c,d] SOPHIE S.W. WANG,[a,b] CHUNG-JUNG LIU,[a,b] KENLY WUPUTRA,[e] KOHSUKE KATO,[f] YEN-LIANG LEE,[g] YING-CHU LIN,[h] MING-HO TSAI,[e] CHIA-CHEN KU,[e] WEN-HSIN LIN,[e] SHIN-WEI WANG,[a,b] SHOTARO KISHIKAWA,[i] MICHIYA NOGUCHI,[j] CHU-CHIEH WU,[c,k] YI-TING CHEN,[c,k] CHEE-YIN CHAI,[c,k] CHEN-LUNG STEVE LIN,[c,e,l] KUNG-KAI KUO,[b,c,l] YA-HAN YANG,[b,e,l] HIROYUKI MIYOSHI,[m] YUKIO NAKAMURA,[j] SHIGEO SAITO,[n,o] KYOSUKE NAGATA,[f] CHANG-SHEN LIN,[e,p] KAZUNARI K. YOKOYAMA [b,e,f,q]

**Key Words.** Bone morphogenetic protein 7 • Gastric cancer • HOXA13 • HoxA transcript at the distal tip • HoxA transcript antisense RNA • iPS-like cells • Jun dimerization protein 2 • Long noncoding RNA • Octamer-binding protein 4

## ABSTRACT

**Reprogramming of cancer cells into induced pluripotent stem cells (iPSCs) is a compelling idea for inhibiting oncogenesis, especially through modulation of homeobox proteins in this reprogramming process. We examined the role of various long noncoding RNAs (lncRNAs)-homeobox protein HOXA13 axis on the switching of the oncogenic function of bone morphogenetic protein 7 (BMP7), which is significantly lost in the gastric cancer cell derived iPS-like cells (iPSLCs). *BMP7* promoter activation occurred through the corecruitment of HOXA13, mixed-lineage leukemia 1 lysine N-methyltransferase, WD repeat-containing protein 5, and lncRNA HoxA transcript at the distal tip (HOTTIP) to commit the epigenetic changes to the trimethylation of lysine 4 on histone H3 in cancer cells. By contrast, HOXA13 inhibited BMP7 expression in iPSLCs via the corecruitment of HOXA13, enhancer of zeste homolog 2, Jumonji and AT rich interactive domain 2, and lncRNA HoxA transcript antisense RNA (HOTAIR) to various *cis*-element of the *BMP7* promoter. Knockdown experiments demonstrated that HOTTIP contributed positively, but HOTAIR regulated negatively to HOXA13-mediated BMP7 expression in cancer cells and iPSLCs, respectively. These findings indicate that the recruitment of HOXA13–HOTTIP and HOXA13–HOTAIR to different sites in the *BMP7* promoter is crucial for the oncogenic fate of human gastric cells. Reprogramming with octamer-binding protein 4 and Jun dimerization protein 2 can inhibit tumorigenesis by switching off BMP7.** STEM CELLS *2017;35:2115–2128*

## SIGNIFICANCE STATEMENT

Reprogramming of the gastric cancer cells is a challengeable approach for therapeutic use. Here we report the successful reprogramming of the human gastric cells into induced pluripotent stem cell–like cells (iPSLCs) using Jun dimerization protein 2 (JDP2) and octamer-binding protein 4 (OCT4). The oncogenic function of Bone morphogenetic protein 7 (BMP7) is switched by long noncoding RNA–HOXA13 axis and lost in the gastric cancer cell-derived iPSLCs. The recruitment of HOXA13–HoxA transcript at the distal tip (HOTTIP) complex and HOXA13–HoxA transcript antisense RNA (HOTAIR) complex to different sites in the *BMP7* promoter is critical for the oncogenic fate of human gastric cells. Thus, reprogramming with OCT4 and JDP2 can inhibit tumorigenic function by switching off BMP7.

## INTRODUCTION

The gene for homeobox protein HOXA13 (*HOXA13*) is located as the most-posterior gene of the *HOXA* cluster in 7p15.2 [1]. Expression of HOXA13 is important for homeostasis in morphogenesis [1]. HOXA13 has a role in cancer promotion of liver stem-like cell lines [2] and the growth of esophageal cancer [3], and is involved in hepatocarcinogenesis [4] and leukemogenesis [5]. Moreover, HOXA13 is a poor prognostic marker for gastric cancer patients [6]. Recently we found that upregulation of HOXA13 plays a critical role in the

[a]Division of Gastroenterology, [b]Center for Stem Cell Research, [c]Department of Medicine, [e]Graduate Institute of Medicine, [h]School of Dentistry; [k]Department of Pathology, [l]Department of Surgery, Kaohsiung Medical University Hospital, Kaohsiung Medical University, Kaohsiung, Taiwan; [d]Department of Internal Medicine, Kaohsiung Municipal Ta-Tung Hospital, Kaohsiung, Taiwan; [f]Department of Infection Biology, Graduate School of Comprehensive Human Sciences, the University of Tsukuba, Tsukuba, Japan; [g]Welgene Biotech. Inc., Taipei, Taiwan; [i]Gene Engineering Division; [j]Cell Engineering Division, RIKEN BioResource Center, Tsukuba, Ibaraki, Japan; [m]Department of Physiology, Keio University School of Medicine, Shinanomachi, Tokyo, Japan; [n]School of Science and Engineering, Teikyo University, Utsunomia, Tochigi, Japan; [o]Saito Laboratory of Cell Technology, Yaita, Tochigi, Japan; [p]Department of Biological Sciences, National Sun Yat-sen University, Kaohsiung, Taiwan; [q]Department of Molecular Preventive Medicine, Graduate School of Medicine, The University of Tokyo, Tokyo, Japan

Correspondence: Chang-Shen Lin, Ph.D., Graduate Institute of Medicine, Kaohsiung Medical University, 100 Shih-Chuan 1st Road, San Ming District, Kaohsiung 807, Taiwan. Telephone: +886-7-312-1101, ext. 2136; Fax: +886-7-313-3849; e-mail: changshen.lin@gmail.com; or Kazunari K. Yokoyama, Ph.D., Graduate Institute of Medicine, Center of Stem Cell Research, Center of Environmental Medicine, Kaohsiung Medical University, 100 Shih-Chuan 1st Road, San Ming District, Kaohsiung 807, Taiwan. Telephone: +886-7-312-1101, ext. 2729; Fax: +886-7-313-3849; e-mail: kazu@kmu.edu.tw

Received November 25, 2016; accepted for publication July 15, 2017; first published online in STEM CELLS *EXPRESS* August 7, 2017.

http://dx.doi.org/10.1002/stem.2674

tumorigenesis of gastric cancer by comparing the nontumorigenic gastric cell line CSN and its derivative cancerous subline CS12 [7].

HOXA13 is reported to directly control the expression of bone morphogenetic protein 7 (BMP7) via binding to its enhancer element [8, 9]. BMP7 is a multifunctional growth factor belonging to the transforming growth factor beta superfamily. In addition to its function in bone formation and cartilage development, BMP7 is relevant in cell proliferation, apoptosis, and organ regulation and repair. In cancer, BMP7 behaves as an oncogene [10] or anti-oncogene [11] depending on ligands and cell types [12].

The long noncoding RNA (lncRNA) *HOXA* transcript at the distal tip (HOTTIP), located at the 5′-end of the *HOXA* cluster, is expressed significantly in anatomically distal human fibroblasts [13]. The interaction of the HOTTIP and WD repeat-containing protein 5 (WDR5)/mixed-lineage leukemia 1 lysine N-methyltransferase (MLL1 also known as histone-lysine N-methyltransferase 2A or KMT2A) in Tithorax complex enhances histone H3 lysine 4 trimethylation (H3K4me3) to activate the expression of 5′-*HOXA* genes including *HOXA13* [14, 15]. Increased HOTTIP expression is a negative prognostic factor in some cancers [16] and promotes tumor progression and drug resistance by regulating HOXA13 in pancreatic cancer [17]. Another lncRNA HOTAIR is expressed from the posterior region of the *HOXC11–12* cluster and is implicated in cancer development. HOTAIR interacts with enhancer of zeste homolog 2 (EZH2), suppressor of zeste 12 homolog subunit (SUZ12) in Polycomb repressive complex 2, and lysine demethylase 1A (LSD1 or KDM1A) to mediate repressive histone modifications at H3K27 and H3K4 at posterior *HOXD* locus [18, 19]. Thus, the actions of HOTTIP and HOTAIR to *HOXA13* and *HOXD10* loci are *cis* and *trans*, respectively [14, 15, 18, 19]. However, to our knowledge no common targets, which are regulated by both lncRNAs are present previously and the mechanistic regulation of the lncRNAs-HOX axis on their target remains to be clarified [20].

We have shown that the Jun dimerization protein 2 (JDP2) is a modulator of wingless-related integration site signaling pathway [21] and works together with octamer-binding protein 4 (OCT4) for the reprogramming of medulloblastoma to generate induced pluripotent stem cell (iPSC)-like cells (iPSLCs) [22]. Liu et al. [23] also reported that JDP2 reprograms the somatic cells into the iPSCs through the five non-Yamanaka factors (Id1, Jhdm1b, Lrh1, Sall4, and Glis1). Thus, JDP2 is a critical factor for the determination of stemness. Here, we used iPSC technology [24] with JDP2 and OCT4 to reprogram CS12 gastric cancer cells to generate induced pluripotent cancer cells [25, 26], and found a reduced tumorigenicity in CS12-derived iPSLCs, suggesting that reprogramming of CS12 cells seems to abrogate the oncogenic function of HOXA13 in CS12 cells [7]. Mechanically, although the expression of HOXA13 was increased in both CS12 cells and iPSLCs, HOXA13 behaved as an oncogene in CS12 but acted as a tumor suppressor in iPSLCs through working with HOTTIP and HOTAIR to up- and down-regulate BMP7 expression, respectively. Knockdown of HOTTIP and BMP7 in CS12 cells decreased cancerous features but downregulation of HOTAIR in iPLSCs promoted cell proliferation. These results suggest that networking between HOXA13 and lncRNAs can manipulate the oncogenic expression of BMP7 in human gastric cancer cells.

## Materials and Methods

### Cell Lines, Animals, Antibodies

Human gastric normal cells CSN and cancerous CS12 cells were cultured as described elsewhere [27]. 293T, and mouse embryonic fibroblasts (MEFs) were obtained from the RIKEN Cell Bank (Tsukuba, Ibaraki, Japan, http://cell.brc.riken.jp/en/) and cultured in Dulbecco's modified Eagle's minimal essential medium (DMEM; Gibco, Carlsbad, CA, https://www.thermofisher.com) supplemented with 10% charcoal-stripped fetal bovine serum (FBS; Gibco) with or without 1% penicillin and streptomycin (Gibco) as described elsewhere [7]. The animal welfare guidelines for the care and use of laboratory animals were approved by the Animal Care Committee of the RIKEN BioResource Center in Japan, the National Laboratory of Animal Center and the Kaohsiung Medical University in Taiwan. All antibodies used in this work are listed in Supporting Information Table S1.

### Plasmids, Small Interference RNA, and Short Hairpin RNA Lentivirus

The human HOXA13 and BMP7 cDNAs were obtained from the RIKEN DNA Bank (IRAK168L10; Tsukuba, Ibaraki, Japan, http://dna.brc.riken.jp/) and were inserted into pcDNA3 (ThermoFisher Scientific, Waltham, MA, https://www.thermofisher.com), pPyCAG-GFP, or pPyCAG-IP [27], to generate expression plasmids for cancer or stem cells. *BMP7* promoter [–1,712 nucleotide (nt) to +110 nt] was obtained from ActiveMotif (NM000522.4; Carlsbad, CA, https://www.activemotif.com/) and was inserted into pGL4 luciferase vectors (Promega, Madison, WI, https://www.promega.com). The mutations of HOX binding sites (S1 to S3) at *BMP7* promoter were generated by polymerase chain reaction using the primers of 5′-CTTCGGAAGTAGCAGGCGCGGTGGA-3′ (S1), 5′-GCGTCAAGTGATAGCGTGAGTGAGTT-3′ (S2), and 5′-GTA CCGAGCCTAGCCTAACTCCCTA-3′ (S3). All constructs were confirmed by DNA sequencing. The short hairpin RNA (shRNA) lentiviruses were generated in 293T cells cotransfected with pCA G-HIVgp-IN-D64V, pCMV-VSV-G-RSV-Rev, or pCMV-dR8.91, or pCMV-d8.74pSPAX2 or VSVG/pMD2G, and TRCN0000355645 or TRCN0000355646 (c-*JUN*), TRCN0000015405 or TRCN0000015406 (*HOXA13*, Academia Sinica, Taipei, Taiwan, http://rnai.genmed.sinica.edu.tw), PLKO.1-GFP (No. 30323; Addgene, Cambridge, MA, https://www.addgene.org) or scrambled control shRNA (Sigma-Aldrich, St. Louis, MO, https://www.sigmaaldrich.com) [7]. Virus was purified at 72 hours after post-transfection as described [28]. The CS12 cells ($1 \times 10^6$) were infected with virus at a multiplicity of infection (MOI) of 2 or 4. After cultivation for 3 days, cells were injected into severe combined immunodeficiency (SCID) mice ($5 \times 10^6$ cells/spot) as described elsewhere [29]. Lentiviruses for human BMP7-shRNA (SV-39748) and HOXA13-shRNA (TR312365, TR312365) were obtained from Santa Cruz Biotech. (Dallas, TX, https://www.scbt.com) and OriGene (Rockville, MD, http://www.origene.com). For small interference RNA (siRNA)-mediated gene knockdown, cells were transfected with siRNA (ThermoFisher Scientific) against *BMP7* (s2035, s2036, s2037), *HOXA13* (s6785, s6786, s6787), *HOTTIP* (n509686, n509687), *HOTAIR* (n272221, n272230), *c-JUN* (s7659) [29], *HOTAIRM1* (n507509, n507510), or negative control pool (s43418, s43420; Dharmacon, D-001810–10-05) using Lipofectamine RNA iMAX reagents (ThermoFisher Scientific). The effects on gene silencing were examined after 48 hours of incubation.

### Generation of iPSLCs From Human Gastric Cancer Cell Line CS12

The CS12 gastric cancer cells ($5 \times 10^5$) were transfected with *OCT4* and *JDP2* by electroporation as described elsewhere [30, 31]. The cells were then selected with G418 (100 μg/ml) for 2 days, and replated onto mitomycin C-treated MEFs in the standard iPS medium (DMEM [Gibco] supplemented with 10% FBS and antimycotics-antibiotics [AM-AB; Gibco] plus human leukemia inhibitoy factor [LIF; 10 ng/mL, ThermoFisher Scientific]) [29, 31] for 2–3 weeks to obtain reprogrammed iPSLCs. Alternatively, recombinant lentiviruses CSIV-CMV-MCS-IRES2-Venus-encoding human OCT4 and JDP2 were generated using 293T cells. CS12 cells ($5 \times 10^4$) were infected with the lentiviruses (MOI = 2) and incubated for 1 week in iPS medium with LIF as described above. Thereafter, cells were transferred onto mitomycin C-treated MEFs in iPS medium plus human LIF (10 ng/ml) to obtain reprogrammed iPSLCs.

### Cell Proliferation, BrdU-Incorporation, and Colony Assay

The numbers of living cells were quantitated using a trypan blue dye-exclusion assay [21, 29]. To analyze the cell cycle, serum-starved cells were stimulated with 15% FBS and then labeled with 10 μM BrdU (Sigma-Aldrich) for 1 hours, trypsinized and fixed overnight with 70% ethanol at 4°C. The fixed cells were incubated in 2M HCl for 1 hours at room temperature, neutralized with 0.1 M $Na_2B_4O_5(OH)_4.8H_2O$, stained by BrdU antibody (BD Bioscience, San Jones, CA, http://www.bdbiosciences.com) at room temperature for 2 hours, followed by Alexa 488-conjugated secondary antibody at room temperature for 30 minutes. DNA was stained with propidium iodide (PI; 5 μg/ml). Cell samples were analyzed with EPICS XL-MCL flow cytometer (Beckman Coulter, Miami, FL, https://www.beckmancoulter.com). To quantitated the cells in S phase, the BrdU Labeling and Detection Kit (Sigma-Aldrich) was used [29]. For the colony-formation assay, cells were plated in duplicate at $5 \times 10^2$ or $5 \times 10^3$ cells/10 cm gelatin-coated dish. Two weeks later, colonies with a diameter $>2$ mm were counted after staining with Giemsa staining solution (Wako Chemicals, Tokyo, Japan, http://www.wako-chem.co.jp/english/).

### Teratoma, Tumor Formation, and Immunohistochemistry

CS12 and CS12iPSLCs were injected subcutaneously into the dorsal flank of SCID mice as described [7, 29]. Tumor size was measured once or twice a week using a caliper. Tumor volume was estimated according to the formula: volume ($cm^3$) = ($L \times W^2$)/2, where L and W are the length and width of the tumor, respectively. The teratomas were fixed in 4% paraformaldehyde overnight and embedded in paraffin. Sections were stained with hematoxylin and eosin.

### Alkaline Phosphatase, Immunocytochemistry, and Karyotyping

Alkaline phosphatase activity measurement and immunocytochemistry were performed as described elsewhere [29, 30]. Chromosome spreads for karyotyping were prepared using a conventional air-drying technique. GTG (G-banding) staining was performed as described elswewhere [32].

### Migration, Invasion, and Chemoresistance Assays

Cells ($1 \times 10^4$ cells) resuspended in DMEM without FBS were seeded in the upper Transwell with or without Matrigel (1 mg/ml, Corning, NY, https://www.corning.com) as described elsewhere [29]. The lower plate contained DMEM plus 10% FBS. Three days later, the cells moved to downside of Transwell were fixed with 4% formaldehyde, stained with 1% crystal violet, and counted under a microscope. Regarding chemoresistance assay, cells were seeded in 96-well plates for 24 hours and then treated with a serial mixture of cisplatin, 5-fluorouracil, and doxorubicin for additional 48 hours. Cell viability was examined using the MTT assay as described elsewhere [21, 29].

### Western Blotting

Western blotting was conducted as described elsewhere [7, 21]. Briefly, cell lysates were prepared in SDS sample buffer or Triton X-100 lysis buffer (10 mM HEPES, pH 7.8, 5% glycerol, 1% Triton X-100, 5 mM EDTA, 50 mM NaF, 20 mM β-glycerophosphate, 50 μg/ml aprotinin, 100 μM leupeptin, 25 μM pepstatin, 1 mM $Na_3VO_4$, and 1 mM PMSF), subjected to SDS–PAGE, and electrotransferred onto a polyvinylidene difluoride membrane (Merck Millipore, Billerica, MA, https://www.merckmillipore.com). After antibody incubation, ECL immunodetection was performed. Results were analyzed using a ChemiDoc XRSPlus analyzer (Bio-Rad, Hercules, CA, http://www.bio-rad.com).

### Reverse Transcriptase PCR and Quantitative Polymerase Chain Reaction

Total RNA was extracted from cells using the TRIzol reagent (ThermoFisher Scientific). RNA was reverse transcribed to cDNA using a reverse transcription kit (Promega). PCR was performed using the GoTaq Green Master Mix (Promega). Quantitative polymerase chain reaction (qPCR) was performed using the QuantiFast SYBR Green PCR kit (Qiagen, Gaithersburg, MD, https://www.qiagen.com) as described elsewhere [7, 21]. β-actin and GAPDH were used as internal controls. Primer sequences are listed in Supporting Information Tables S2–S4.

### Transient Transfection and Luciferase Assay

Transient transfection and the luciferase assay were performed as described elsewhere [7, 21, 33–35]. Cells were plated into each well of a 12-well plate and cultured for 24 hours. The cells were then cotransfected with indicated amounts of various effector constructs and BMP7-promoter-luciferase reporters using Lipofectamine 2000 (Invitrogen). The total amount of transfected DNA was kept constant at 1 μg per well by the addition of pBluescript. After 48 hours or the indicated period of incubation, cells were harvested for luciferase activity assay using Dual-Luciferase Reporter Assay System (Promega) and an illuminometer (Berthold Technologies, Bad Wildbad, Germany, https://www.berthold.com).

### Chromatin Immunoprecipitation Assay

Chromatin immunoprecipitation (ChIP) assay was performed as described elsewhere [7, 29, 33]. The immunoprecipitated protein–DNA complexes were washed twice with binding buffer (10 mM HEPES, pH 7.9, 10 mM Tris-HCl, pH 7.9, 12.5% glycerol, 0.25% NP-40, 0.5% Triton X-100, 0.24 M NaCl,

0.75 mM $MgCl_2$, 1.1 mM EDTA, and protease inhibitor mixture) and then washed twice with Tris-EDTA buffer (10 mM Tris-HCl, pH 7.9, and 1 mM EDTA). The protein–DNA complexes were disrupted with proteinase K (Sigma-Aldrich) at pH 6.8. DNA was extracted with phenol and chloroform, precipitated in ethanol, and analyzed by real-time PCR using the Power SYBR Green Master Mix (Invitrogen). The PCR conditions consisted of 1 cycle of 2 minutes at 50°C and 1 cycle of 10 minutes at 95°C followed by 40 cycles of 95°C for 15 seconds, and 55°C−60°C for 60 seconds. The primers used in these experiments are shown in Supporting Information Table S5.

### RNA Immunoprecipiotation Assay

RNA immunoprecipiotation (RIP) assay was performed as described elsewhere [36]. Cells were lysed in RIP lysis buffer (10 mM HEPES, pH 8.0, 40 mM KCl, 3 mM MgCl2, 5% glycerol, 2 mM DTT, 0.5% sodium deoxycholate, 100 unit/ml RNase inhibitor and protease inhibitors) and the resulted cell lysates (1 mg) were incubated with HOXA13 antibody for 2 hours, followed by 1 mg/ml tRNA-precleared protein A/G beads for another 2 hours. The immunoprecipitates were washed by RIP lysis buffer and resuspended in TRIzol reagent (ThermoFisher Scientific) to extract the immunoprecipitated RNA for reverse transcription and qPCR.

### Statistical Analyses

The data are presented as the mean ± SEM from 3–6 experiments. Difference between two and multiple experimental groups was assessed using two-tailed Student's *t* tests and one-way ANOVA, respectively. Survival analysis was performed using the Kaplan–Meier method with log-rank test. $p < .05$ was considered statistically significant.

## Results

### Comparative Expression of Stemness Genes in iPSLCs and CS12 Cells

We used transcription factors, JDP2 and OCT4, to induce reprogramming and generate iPSCs as described previously [22], because it was not feasible to use the standard four Yamanaka factors [24] to generate stem cell-like colonies (data not shown) in the normal human gastric mucosa cell line CSN and its derived CS12 cancer cells [7]. Three weeks after electroporation of JDP2 and OCT4, small, packed, domed iPSC-like colonies were detected (Fig. 1A). The number of colonies with a typical iPSC phenotype increased over time by repetitive passage. When iPSLCs were cultured for more than 4 weeks, the CS12iPSLCs displayed strong alkaline phosphatase activity (Fig. 1A). qPCR revealed that the endogenous expression of OCT4 and KLF4 in CS12iPSLCs increased about 3.4- and 5.3-fold, respectively, but NANOG and ESRRB were repressed by 50% compared with CS12 cells (Fig. 1B). Endogenous expression of JDP2 and p53 was also reduced by about 50% in CS12iPSLCs (Fig. 1B). RNA sequence analysis showed that the primitive germ layer markers such as SOX1 (ectoderm), SOX17 (endoderm), and T (mesoderm) were not changed between CS12 and CS12iPLSCs (Supporting Information Fig. S1A); by contrast, the pluripotent markers ESRRB and KLF2, but not REX1 and SALL4, were reduced by 30%–45% in CS12iPSLCs (Supporting Information Fig. S1A). Immunofluorescence staining confirmed the expression of stemness markers (OCT4, SOX2, NANOG, SSEA4, Tra-1–60, Tra-1–81) in CS12iPSLCs (Fig. 1C). To confirm the pluripotency [29], we transferred CS12iPSLCs into SCID mice to generate teratomas, which showed two germ layers such as endoderm and ectoderm (Fig. 1D). However, three germ layers were not observed in any instance. These results suggest that CS12iPSLCs were not fully pluripotent. The karyotype analysis showed no changes of chromosomes in CS12iPSLCs (Supporting Information Fig. S1B).

### CS12iPSLCs Exhibited Reduced Tumorigenicity In Vivo

To compare the tumorigenicity of CS12 and CS12iPSLCs, we injected these cells subcutaneously into SCID mice. One month after injection, tumors generated by CS12 cells expanded to 2.5 $cm^3$, which was 10 times the size of those generated by CS12iPSLCs (Fig. 1E). Both sizes and weights of tumors generated by CS12iPSLCs were smaller than those of CS12 cells (Fig. 1F, 1G). CS12iPSLCs-derived xenografts exhibited reduced numbers of necrotic cells and the cells with large nucleus and mitosis (Fig. 1E). Thus, CS12iPSLCs exhibited reduced tumorigenicity in vivo when compared with CS12 cells.

### Decreased Cell Proliferation, Colony Formation, Cell Migration and Invasion, and Drug Resistance in CS12iPSLCs

To verify the difference in oncogenic activity between CS12 and CS12iPSLCs, cell proliferation, colony formation, cell migration, invasion, and drug resistance were examined. The CS12 cells proliferated more rapidly than CS12iPSLCs and CSN cells (Fig. 2A). The colony-forming ability of CS12 cells was twofold higher than that of CS12iPSLCs (Fig. 2B). Cell cycle analysis of bromodeoxyuridine (BrdU)-labled cells and BrdU ELISA assay confirmed that cell proliferation of CS12iPSLCs was reduced (Fig. 2C). No increase in apoptosis was found in CS12iPSLCs (Supporting Information Fig. S1C). Transwell assays demonstrated that both the migration and invasion efficacies of CS12 cells were higher than those of CS12iPSLCs and CSN cells (Fig. 2D), which were consistent with the increased expression of Snail 1 family transcriptional repressor 1/2 (Snail1/2), Matrix metalloproteinase 2 (MMP2), Vimentin, and with the decrease of E-CADHERIN in CS12 cells (Supporting Information Fig. S1D, S1E). To examine the drug resistance, cell viability was measured by incubating cells with a mixture of three conventional drugs for chemotherapy: 5-fluorouracil, cisplatin, and doxorubicin. CS12 cells showed greater resistance to these drugs than CS12iPSLC and CSN cells (Fig. 2E), demonstrating the increased chemoresistance of CS12 cells.

### Enhanced Expression of HOXA13 in CS12iPSLCs and CS12 Cells

We previously reported that several *HOXA* genes were upregulated in CS12 when compared with CSN cells [37] and upregulated HOXA13 contributed to the tumorigenicity of CS12 cells [7]. Here, we found that the expressions of HOXA4, 5, 7, and 9 were decreased in CS12iPSLCs when compared with

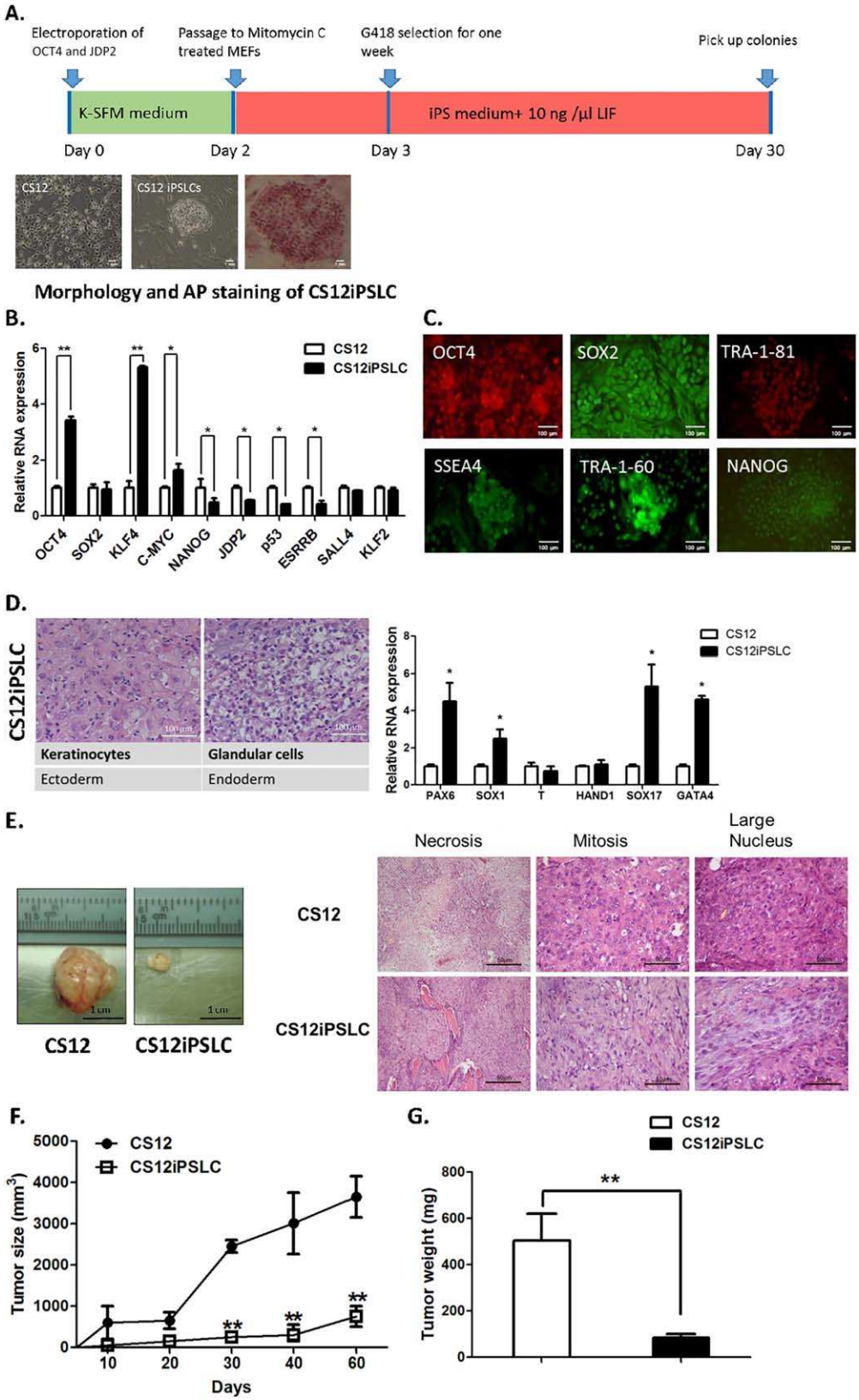


**Figure 1.** Generation and tumorigenicity of iPSLCs from CS12 gastric cancer cells. **(A)**: Schematic representation of iPSLCs generation from CS12 cells by OCT4 and JDP2. Morphology (CS12 and CS12iPSLCs) and alkaline phosphatase staining (CS12iPSLCs) are shown (magnification, ×100). **(B)**: Expression of stemness genes analyzed by quantitative reverse transcriptase PCR (RT-PCR). The plot shows the mean ($n = 5$) ± SEM (*, $p < .05$; **, $p < .01$). **(C)**: Immunocytochemical analysis of pluripotency markers in CS12iPSLCs (magnification, ×200). **(D)**: (Left panel) Pluripotency of CS12iPSLCs. Teratomas that were generated by the transplantation of CS12iPSLCs into severe combined immunodeficiency (SCID) mice were examined by immunohistochemistry, which shows differentiation of the ectoderm (keratinocytes) and endoderm (glandular cells). White bar, 100 μm. (Right panel) Expression of differentiation marker genes were examined by quantitative RT-PCR. The plot shows the mean ($n = 5$) ± SEM (*, $p < .05$). **(E)**: Tumor formation of subcutaneously injected CS12 and CS12iPSLCs in SCID mice. Tumor was sectioned and stained with hematoxylin and eosin (scale bar, 50 μm). **(F)**: Tumor sizes of CS12 and CS12iPSLCs. The plot shows the mean ($n = 5$) ± SEM (**, $p < .01$). **(G)**: Tumor weight of CS12 and CS12iPSLCs. Plot shows the mean ($n = 5$) ± SEM (**, $p < .01$). Abbreviations: MEFs, mouse embryonic fibroblasts iPS, induced pluripotent stem; LIF, leukemia inhibitoy factor; iPSLCs, induced pluripotent stem cell-like cells; JDP2, Jun dimerization protein 2; OCT4, octamer-binding protein 4.

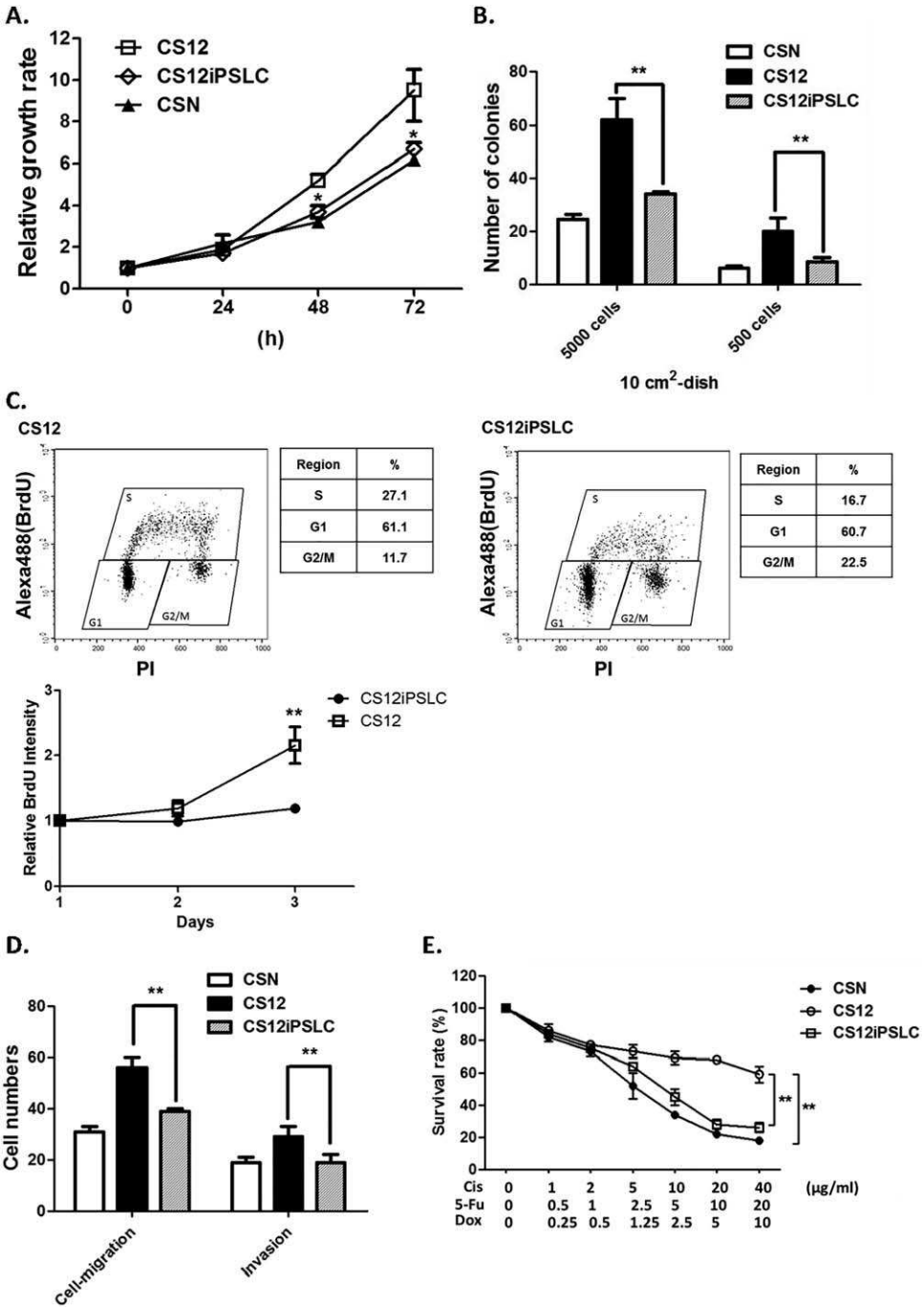


**Figure 2.** Comparison of in vitro cancer features of CSN, CS12, and CS12iPSLCs. **(A)**: Cell growth of CSN, CS12, and CS12iPSLCs was determined using trypan blue dye-exclusion test ($n = 5$). **(B)**: Colony formation of CSN, CS12, and CS12iPSLCs. Cells were plated in gelatin-coated dishes and colonies with a diameter $> 2$ mm were counted 2 weeks later. **(C)**: (Upper panels) BrdU incorporation assay. *x*-axis indicates DNA contents (PI) and *y*-axis indicates BrdU intensity. Cell populations at G1, S, and G2/M phases were shown in Tables (Lower panel), BrdU-incorporation and ELISA assay using the BrdU Labeling and Detection Kit I (Sigma-Aldrich). Data are presented as means ($n = 3$) $\pm$ SEM, **, $p < .01$. **(D)**: The degrees of invasion and migration were analyzed by Transwell with and without Matrigel, respectively. **(E)**: The drug-resistance capacities of CSN, CS12, CS12iPSLCs were demonstrated by the survival rates of cells treated with 5-Fu, Cis, and Dox. Data are presented as means ($n = 3$) $\pm$ SEM, *, $p < .05$; **, $p < .01$. Abbreviations: 5-Fu, 5-fluorouracil; BrdU, bromodeoxyuridine; Cis, cisplatin; Dox, doxorubicin; iPSLCs, induced pluripotent stem cell-like cells; PI, propidium iodide.

CS12 cells (Fig. 3A; Supporting Information Figure S2A). Unexpectedly, HOXA13 was further increased in CS12iPSLCs (Fig. 3A, 3B; Supporting Information Figure S2A), implying that other factors might be involved in determining the oncogenic activity of HOXA13.

To clarify the effects of HOXA13 on the different tumorigenicity between CS12 and CS12iPSLCs, HOXA13-knockdown CS12 cells (Fig. 3C), and CS12iPSLCs (Fig. 3E) were inoculated into SCID mice to compare xenograft formation ability. Knockdown of HOXA13 in CS12 cells decreased tumor

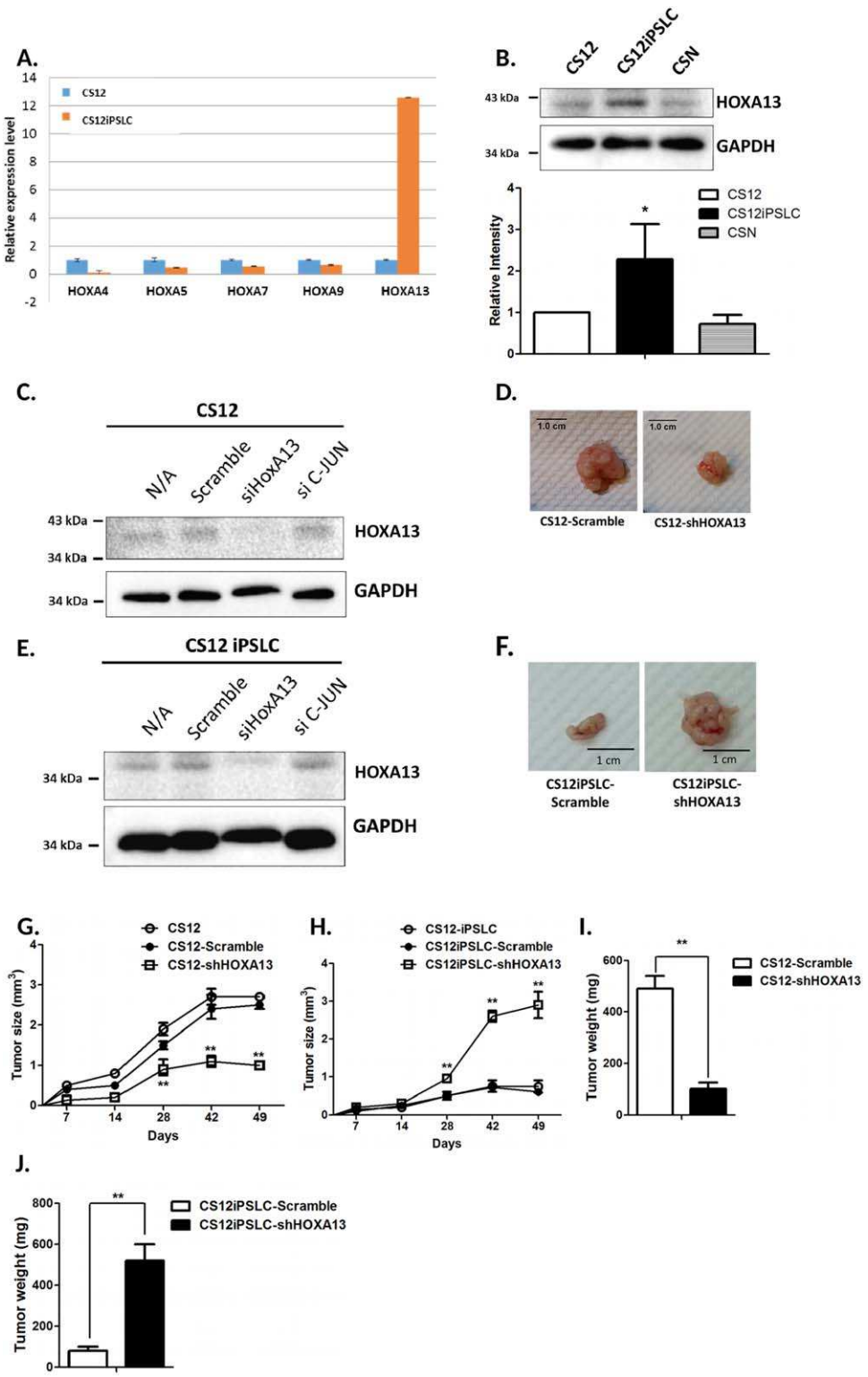


**Figure 3.** Role of HOXA13 in tumor formation of CS12 and CS12iPSLCs xenografts. **(A)**: Comparative mRNA expressions of *HOXA* family genes in CS12 and CS12iPSLCs were examined by quantitative reverse transcriptase PCR. The data are presented as mean ± SEM. Relative expression of HOXA mRNA in CS12 cells was set as one. **(B)**: Comparative expression of HOXA13 proteins in CSN, CS12, and CS12iPSLCs. The exposure time is 100 seconds. Data are presented as means ($n = 3$) ± SEM, *, $p < .05$. **(C)**: Expression of HOXA13 was examined by Western blot in CS12 cells treated with siRNA against *HOXA13, c-JUN,* or scramble control. The exposuire time was 50 seconds. **(D)**: The effect of HOXA13 knockdown on tumor growth of CS12 xenografts. **(E)**: Comparative expression of HOXA13 was examined by Western blot in CS12iPSLCs treated with siRNA against *HOXA13*, *c-JUN,* or scramble control. The exposure time is 50 seconds. (F): The effects of HOXA13 knockdown on tumor growth of CS12iPSLCs xenografts. **(G, H)**: The effects of HOXA13 knockdown on tumor sizes of CS12 (G) and CS12iPSLCs (H) xenografts. (I, J): The effects of HOXA13 knockdown on tumor weights of CS12 (I) and CS12iPSLCs (J) xenografts. All data in (G–J) were derived from six independent experiments and are presented as mean ± SEM (**, $p < .01$). Abbreviation: iPSLCs, induced pluripotent stem cell-like cells.

formation and tumor weight (Fig. 3D, 3G, 3I). In contrast, HOXA13-knockdown CS12iPSLCs increased tumor size and tumor weight (Fig. 3F, 3H, 3J). These data support the notion that HOXA13 in conjunction with some unspecified factors determined the tumorigenicity of CS12 cells and CS12iPSLCs.

### Differential Expressions of BMP7 and lncRNAs were Critical to Determine the Tumorigenicity of CS12 Cells and CS12iPSLCs

To further characterize the differences between CS12 and CS12iPSLCs, we examined the expression profiles of CS12 and CS12iPSLCs using RNA sequencing and confirmed that BMP7, a known HOXA13 target [8, 9], was upregulated in CS12 compared with that in CS12iPSLCs (Fig. 4A; Supporting Information Fig. S3B). Expressions of BMP7 protein and phosphorylated SMAD1 protein were indeed upregulated in CS12, suggesting the crosstalk of BMP7-SMAD axis [9] (Supporting Information Fig. S2B). BMP7 might be critical because it was altered significantly in several gene ontology categories, such as stem cancer stem, pluripotent stem progenitors, epithelial-mesenchymal transition (EMT)/mesenchymal-epithelial transition (MET), cytokines, and growth factors (Supporting Information Fig. S3B). Knockdown of HOXA13 but not c-JUN (as a control) in CS12 cells decreased BMP7 protein level (Supporting Information Fig. S3A). Expressions of other HOXA13 targets including BMP2, insulin-like growth factor-binding protein 3 and annexin A2 as well as FGF8 were not changed (Fig. 4A).

We also found the preferential upregulation of HOTTIP in CS12 cells and HOTAIR in CS12iPSLCs, respectively, (Fig. 4B). The expression of another *HOXA* transcript antisense RNA, myeloid-specific 1 (HOTAIRM1) expression was unchanged (Fig. 4B). Because HOTTIP and HOTAIR regulate expression of *HOX* gene clusters, and HOXA13 controls BMP7 expression, we next examine the role of HOTTIP/HOTAIR–HOXA13–BMP7 axis in tumorigenicity by knockdown experiments (Fig. 4C, 4D).

In CS12 cells, siHOTTIP reduced the expression of HOXA13 as reported [6, 12, 14], but siHOTAIR did not affect the expression of HOXA13. By contrast, in CS12iPSLCs, siHOTTIP did not affect the expression of HOXA13, but siHOTAIR decreased the expression of HOXA13 (Supporting Information Fig. S4A). In CS12 cells, knockdown of BMP7 and HOTTIP, but not HOTAIR, decreased cell growth, colony formation, cell migration and invasion activity (Fig. 4E–4H), suggesting that HOTTIP and BMP7 contribute to the tumorigenicity of CS12 cells. Conversely, knockdown of HOTAIR, but not BMP7, in CS12iPSLCs, increased cell growth, colony formation, cell migration, and invasion activity (Fig. 4E–4H), indicating that HOTAIR played a tumor suppressor role in CS12iPSLCs. Knockdown of HOXA13 resulted in a reduced cell growth in CS12 cells but caused an increase of cell proliferation in CS12iPSLCs (Fig. 4E), which was consistent with the results of mouse xenograft model (Fig. 3). The reduced tumorigenicity of CS12iPSLCs was also associated with restored expressions of p53 and several CDK inhibitors including $p16^{Ink4a}$, $p15^{Ink4b}$, $p18^{Inc4c}$, $p21^{Cip1}$, $p27^{Kip1}$, and $p57^{Kip2}$, together with decreased E2F-1 expression in CS12iPSLCs compared with that in CS12 cells (Supporting Information Fig. S4B).

On the other hand, overexpression of BMP7 in CS12iPSLCs increased cell proliferation, colony formation, and cell migration and invasion (Supporting Information Fig. S5A–S5E). The in vivo tumorigenicity of BMP7-transduced CS12iPSLCs showed increased tumor incidence and mortality compared with that of control cells (Supporting Information Fig. S5F, S5G). Blood vessels, giant cells, mitotic cells, and necrosis were also detected significantly in the tumors derived from BMP7-transformed CS12iPSLCs (data not shown).

### Differential Recruitment of HOXA13 to the *BMP7* Promoter at S1 and S2 Sites in CS12 and CS12iPSLCs, Respectively

Given that BMP7 was differentially expressed in CS12 and CS12iPSLCs (Fig. 4A, Supporting Information Fig. S2B, S3B), and was critical for determining the tumorigenicity of both cells (Fig. 4E–4H), and forced expression of BMP7 enhanced tumorigenic features in CS12iPSLCs (Supporting Information Fig. S5), we investigated how BMP7 expression was regulated in both cells. It is known that HOXA13 directly binds to the *BMP7* promoter and induces BMP7 expression [9, 38, 39]. We conducted ChIP assays to examine the binding of HOXA13 to the *BMP7* promoter in CS12iPSLCs and CS12 cells. Computational sequence analysis revealed three putative HOX-binding sites: S1 (–412/–416), S2 (–1,113/–1,117), and S3 (–1,613/–1,617) in the *BMP7* promoter (Fig. 5A) (PROMO3; TRANSFAC v8.3) [40]. The results of ChIP showed that recruitment of HOXA13 to the S1 site was increased in CS12 cells but not in CS12iPSLCs. By contrast, binding of HOXA13 to the S2 site was increased in CS12iPSLCs but not in CS12 cells (Fig. 5A). No significant recruitment of HOXA13, HOXA9, or HOXA7 was found at the S3 site and nonspecific NS site. In addition, ChIP assays demonstrated an elevated trimethylation of lysine 4 on histone H3 (H3K4me3) and an increased recruitment of MLL1/WDR5 at the S1 site in CS12 cells, but not in CS12iPSLCs (Fig. 5B), indicative of activated *BMP7* promoter in CS12 cells. By contrast, increased H3K27me3 and recruitments of EZH2 and jumonji AT-rich interactive domain 2 (JARID2) [41] were found at the S2 site in CS12iPSLCs, but not in CS12 cells (Fig. 5B), explaining the reduced BMP7 expression in CS12iPSLCs. No significant difference in these epigenetic marks was observed at the S3 and NS sites in both cells (Fig. 5B). The expression levels of Polycomb group RING finger complex protein B lymphoma Mo-MLV insertion region 1 homolog (BMI1), EZH2, SUZ12, and JARID2 were significantly higher in CS12iPSLCs than in CS12 cells (Supporting Information Fig. S6). Moreover, an RNA immunoprecipitation experiment [36] demonstrated that the association between HOXA13 and HOTTIP was predominant in CS12; by contrast, HOTAIR-HOXA13 interactioon is evident in CS12iPSLCs (Fig. 5C). These findings suggested that the differential recruitment of HOXA13 was correlated with contrasting epigenetic marks at the S1 and S2 sites of the *BMP7* promoter and conversed expression patterns of BMP7 in CS12 cells and CS12iPSLCs.

### HOXA13 Differentially Upregulates and Downregulates *BMP7* Promoter Activity Through the S1 and S2 Sites, Respectively

To further examine the roles of S1 and S2 sites in HOXA13-mediated BMP7 expression, we cloned *BMP7* promoters, both wild-type and HOX-binding site mutants, into a luciferase reporter plasmid (Fig. 6A) and then cotransfected them with a HOXA13-expressing plasmid into CS12 cells. The results showed that HOXA13 transactivated wild-type and S2- and S3-

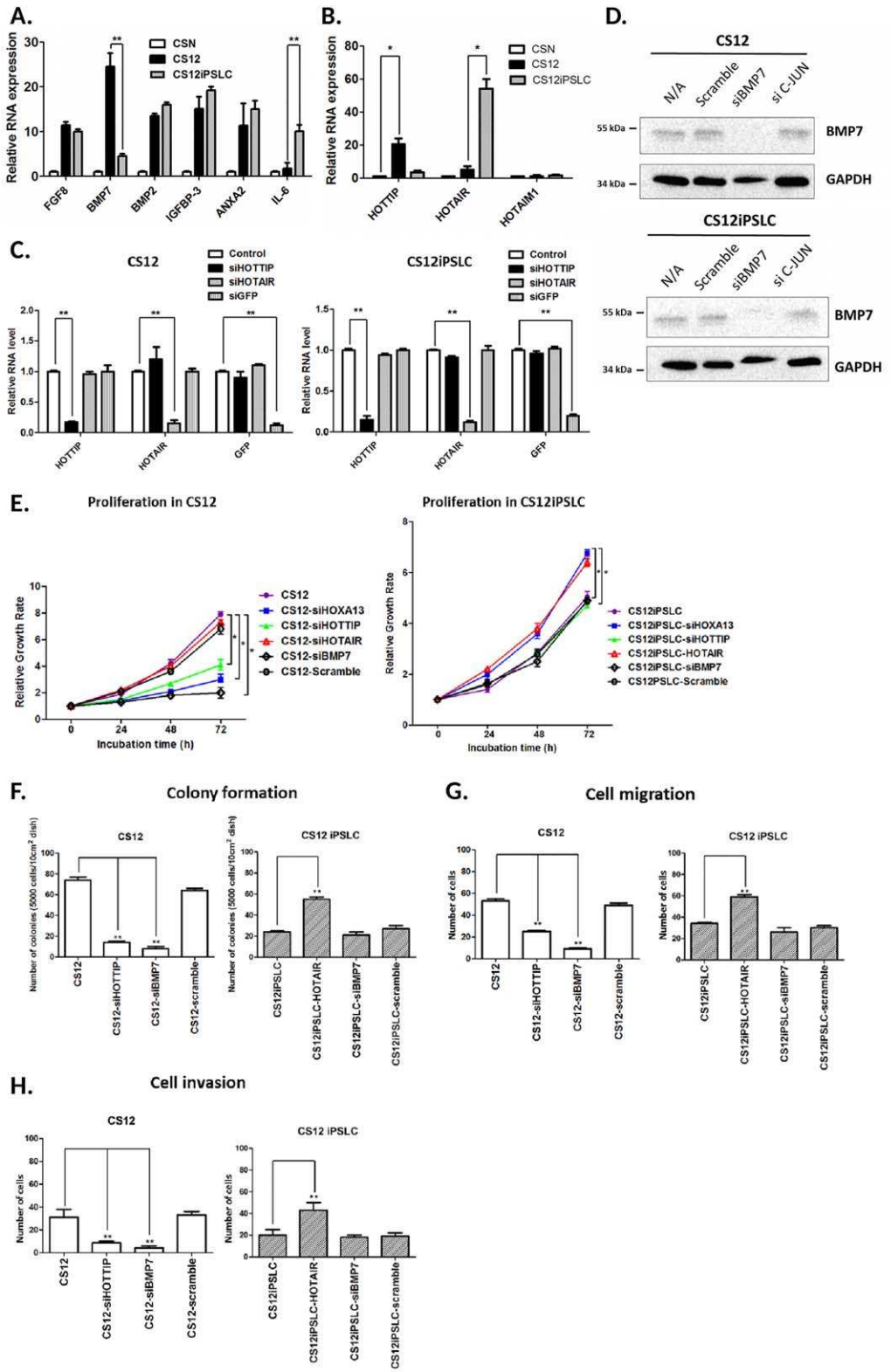


**Figure 4.** Identification of BMP7 and long noncoding RNAs as critical determinants of tumorigenicity. **(A)**: Comparative mRNA expression of FGF8, BMP2, BMP7, IGFBP-3, ANXA2, and IL-6 in CSN, CS12, and CS12 iPSLCs was examined by quantitative reverse transcriptase PCR (RT-PCR). **(B)**: Comparative expression of HOTTIP, HOTAIR, and HOTAIRM1 in CSN, CS12, and CS12iPSLCs was examined by quantitative RT-PCR. **(C)**: Knockdown of GFP, HOTTIP, or HOTAIR by respective siRNAs in CS12 cells (left) and CS12iPSLCs (right). **(D)**: Knockdown of BMP7 was examined by Western blot in CS12 (left) and CS12iPSLCs (right). The exposure time is 100 seconds (left) and 200 seconds (right), respectively. **(E)**: Effect of siRNA against HOXA13, HOTTIP, HOTAIR, or BMP7 on cell proliferation of CS12 (left) and CS12iPSLCs (right) was examined by trypan blue dye-exclusion test. **(F)**: Effect of siRNA against HOTTIP, HOTAIR, or BMP7 on colony formation of CS12 (left) and CS12iPSLCs (right). **(G)**: Effect of siRNA against HOTTIP, HOTAIR, or BMP7 on cell migration of CS12 (left) and CS12iPSLC (right). **(H)**: Effect of siRNA against HOTTIP, HOTAIR, or BMP7 on cell invasion of CS12 (left) and CS12iPSLC (right). All data are presented as mean $\pm$ SEM ($n = 5$; *, $p < .05$; **, $p < .01$). Abbreviations: BMP7, bone morphogenetic protein 7; HOTTIP, HoxA transcript at the distal tip; HOTAIR, HoxA transcript antisense RNA; iPSLCs, induced pluripotent stem cell-like cells.

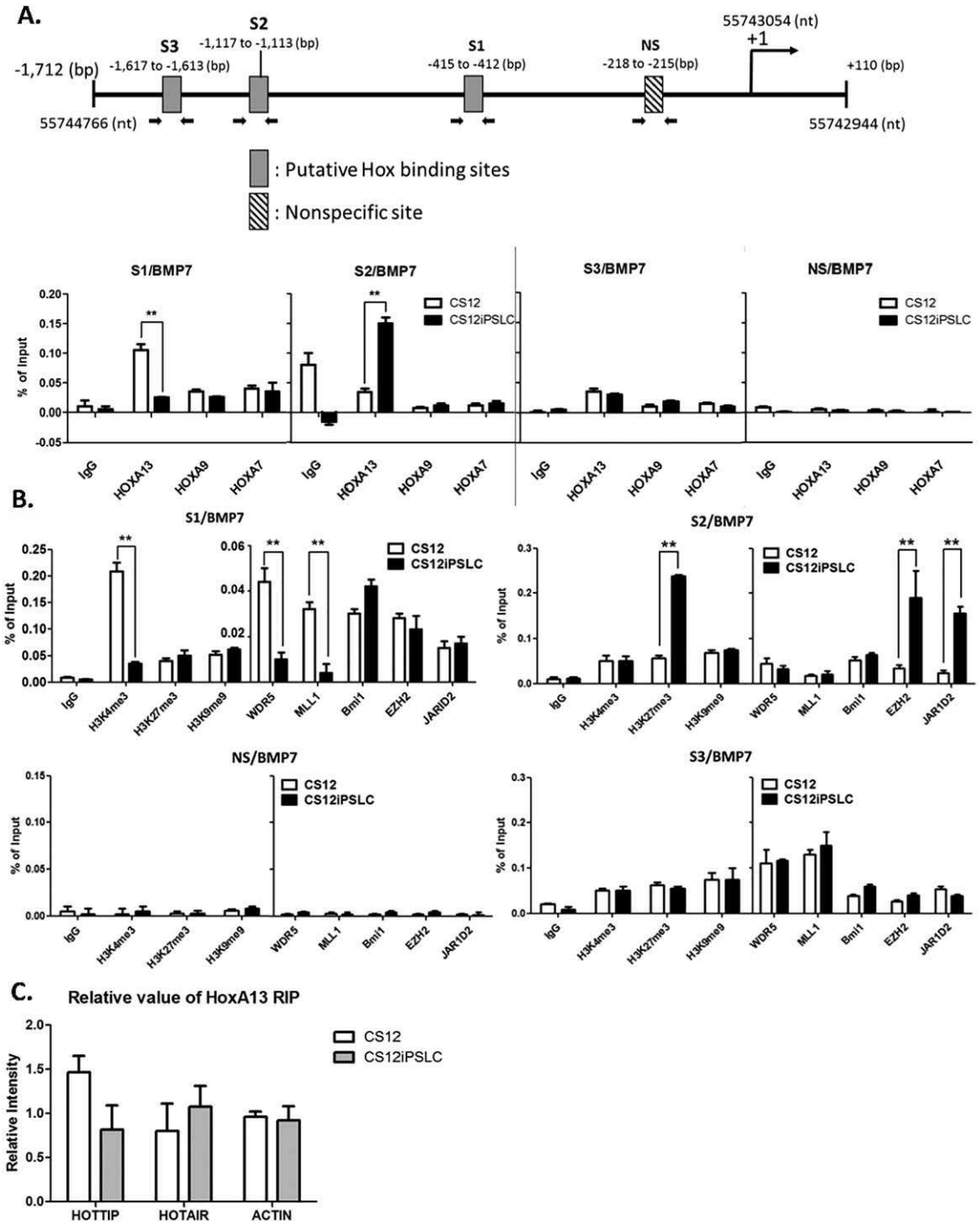


**Figure 5.** Differential epigenetic states of *BMP7* promoter in CS12 and CS12iPSLCs. **(A)**: Schematic representation of *BMP7* promoter and the putative HOX-binding sites: S1, S2, and S3. Q-PCR primers for chromatin immunoprecipitation (ChIP) assay are denoted by arrows, including a NS site. ChIP–qPCR analyses of HOXA7, HOXA9, HOXA13, and IgG (negative control) were performed using CS12 (open bar) and CS12iPSLCs (solid bar) lysates. Input; 5% DNA. **(B)**: ChIP–qPCR analyses using antibodies against methylated histones, WDR5–MLL complex, PRC2 complex, and JARID2 were performed in CS12 and CS12iPSLCs. Input: 5% DNA. The data are presented as mean ± SEM ($n = 5$; **, $p < .01$). **(C)**: RNA immunoprecipitation (RIP) assay. CS12 and CS12iPSLC lysates were incubated with antibody against HOXA13 or control IgG, and then precipitates by protein A/G beads. The RNA in the immunoprecipitates was extrcated using TRIzol and was subjected to quantitative reverse transcriptase PCR to detect the HOXA13-bound HOTTIP, and HOTAIR. β-actin RNA serves as a negative control. The relative intensity of binding was normalized by that of IgG and the data was shown as mean ± SEM ($n = 5$). Abbreviations: BMP7, bone morphogenetic protein 7; HOTAIR, HoxA transcript antisense RNA; HOTTIP, HoxA transcript at the distal tip; iPSLCs, induced pluripotent stem cell-like cells; NS, nonspecific.

mutated *BMP7* promoters comparably, but just marginally induced S1-mutated *BMP7* promoter (Fig. 6B), supporting that HOXA13 induced BMP7 expression through S1 site in CS12 cells. To examine the effect of HOXA13 on *BMP7* promoter in iPSLCs, we used a feasible promoter (pPyCAG) to drive HOXA13 expression in stem cells [35]. The results showed that

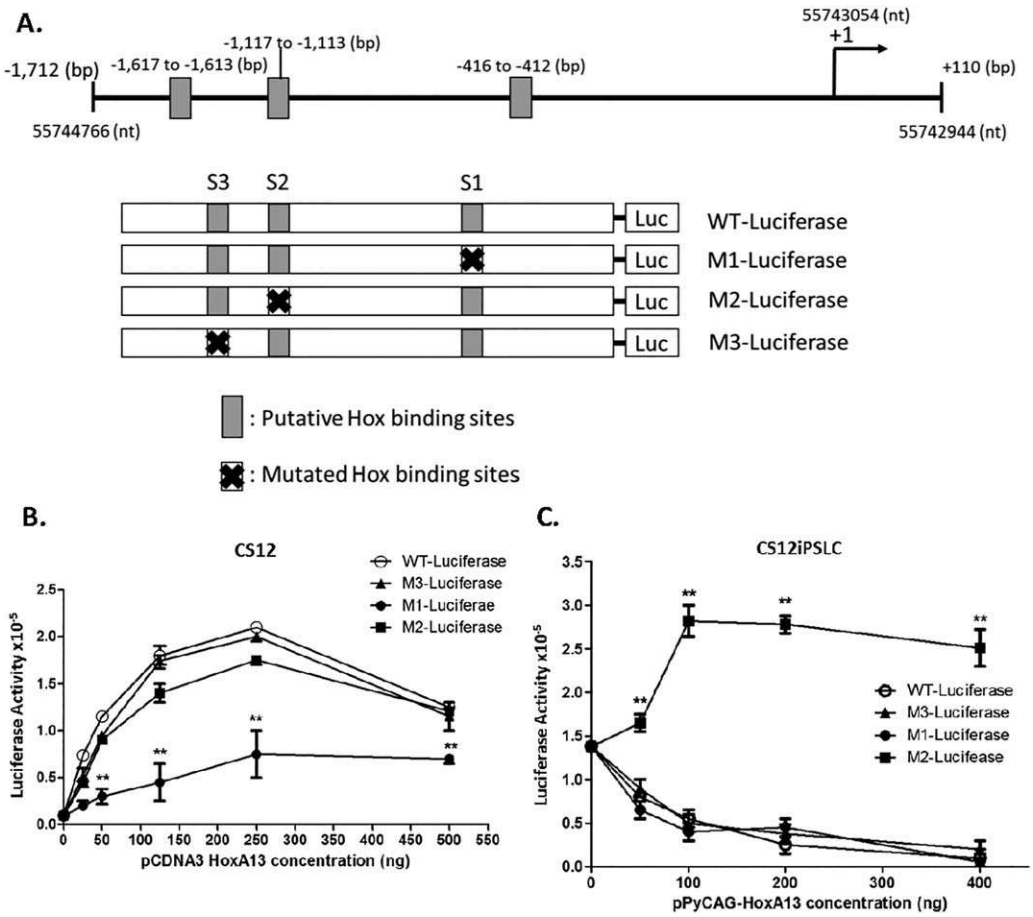


**Figure 6.** HOXA13 regulates *BMP 7* promoter through HOX-binding sites. **(A)**: Schematic representation of *BMP7* promoter luciferase constructs containing WT or mutations at the putative HOX binding sites (S1 to S3). **(B)**: HOXA13 transactivated *BMP7* promoter through S1 site in CS12 cells. **(C)**: HOXA13 repressed *BMP7* promoter through S2 site in CS12iPSLCs. Various *BMP7* promoter luciferase constructs were cotransfected with pcDNA3-HOXA13 into CS12 cells (B) or pPyCAG-FLAG-HOXA13 into CS12iPSLCs (C) for 48 hours, and then the luciferase activity was measured. The data are presented as mean ± SEM ($n = 5$; **, $p < .01$). Abbreviations: WT, wild type; iPSLCs, induced pluripotent stem cell-like cells.

only S2 mutant displayed increased activity but all other mutants and wild type *BMP7* promoter constructs showed significant repression in CS12iPSLCs (Fig. 6C), suggesting that HOXA13 inhibited BMP7 expression through S2 site.

### HOTTIP– and HOTAIR–Differentially Regulated *BMP7* Promoter Activity and the Epigenetic Configurations at S1 and S2 Sites

Because HOTTIP and HOTAIR regulate gene expression through MLL–WDR5 and PRC2–EZH2 complexes, respectively [12, 17, 42], we examined the effects of siHOTTIP and siHOTAIR on the recruitments of MLL–WDR5 and SUZ–EZH2–JARID2 to the *BMP7* promoter in CS12 and CS12iPSLCs. The results showed that knockdown of HOTTIP, but not HOTAIR, reduced H3K4me3 and decreased the recruitment of MLL/WDR5 to the S1 site in CS12 cells (Fig. 7A), suggesting that HOTTIP knockdown might decrease *BMP7* promoter activity. Knockdown of HOTAIR, but not HOTTIP, reduced H3K27me3 and decreased the recruitment of EZH2 and JARID2 to the S2 site of the *BMP7* promoter in CS12iPSLCs (Fig. 7B), indicating that HOTAIR contributed to the suppressive configuration at the S2 site. The knockdown of HOXA13 also showed similar patterns of HOTTIP–MLL–WDR5 axis in CS12 cells and HOTAIR–EZH2–JARID2 axis in CS12iPSLCs (Fig. 7A, 7B). Indeed, knockdown of HOTTIP or HOXA13 decreased *BMP7* promoter activity in CS12 cells (Fig. 7C), while HOTAIR knockdown increased *BMP7* promoter activity in CS12iPSLCs (Fig. 7D). These findings demonstrated that HOTTIP upregulated BMP7 expression in CS12, but HOTAIR suppressed BMP7 expression in CS12iPSLCs, both were involved with HOXA13 (Fig. 7E).

## Discussion

In this study, we reprogrammed the human gastric cancer cell line CS12 using OCT4 and JDP2 to generate CS12iPSLCs (Fig. 1). This technique is useful for cellular reprogramming of somatic cells and cancer cells into stem cells or stem-like cells, which can serve as disease model or a platform for drug screening. Notably, the reprogrammed CS12iPSLCs exhibited less tumor formation capacity in SCID mice when compared with the parental CS12 cells (Fig. 1E–1G), suggesting that reprogramming of cancer cells may be a strategy that could be developed for the future therapy.

Accumulating evidence reveals that high-level expression of BMP7 correlates with increased invasion and metastasis

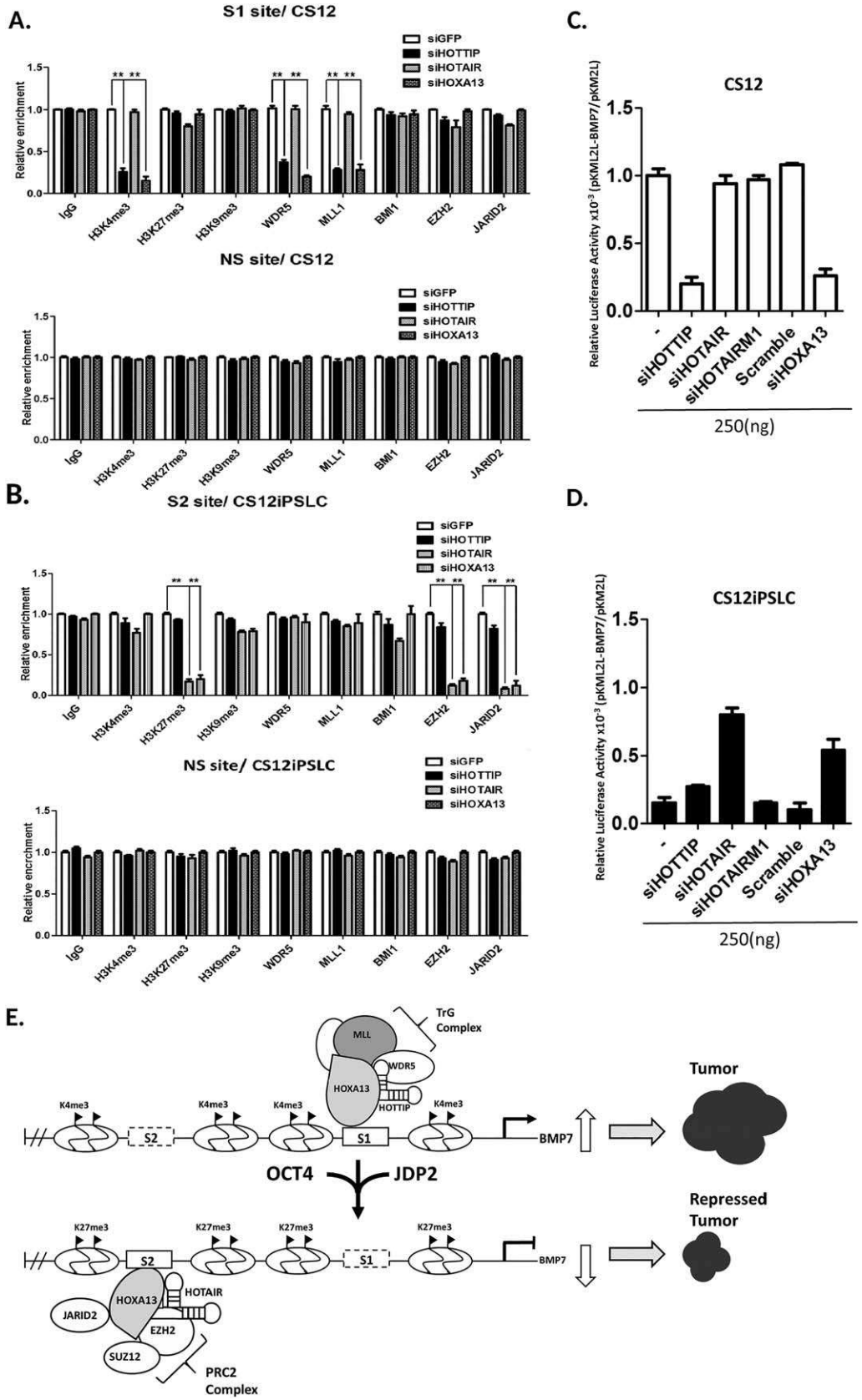


**Figure 7.** Regulation of epigenetic configuration and *BMP7* promoter activity by siRNA against HOTTIP, HOTAIR, and HOXA13. **(A, B)**: Effect of siRNA against GFP, HOTTIP, HOTAIR, and HOXA13 on histone methylations and recruitments of WDR5-MLL1, and PRC2 complexes to the S1 and NS sites in CS12 cells (A) or to the S2 site and NS sites in CS12iPSLCs (B). (**C, D**): Effects of siHOTTIP, siHOTAIR, and siHOXA13 on *BMP7* promoter activities in CS12 (C) and CS12iPSLCs (D), respectively. The untreated *BMP7* promoter activity in CS12 cells was assigned as one. The data are presented as mean $\pm$ SEM ($n = 5$; **, $p < .01$). **(E)**: Schematic representation of the role of HOXA13-HOTTIP axis and HOXA13-HOTAIR axis on the *BMP7* promoter in CS12 and CS12iPSLCs. K4me3; histone H3K4me3, K27me3; histone H3K27me3. Trithorax complex is composed of MLL, WDR and other components including JARID2. Polycomb repressive complex 2 is composed of SUZ12, EZH2 and other components. Abbreviations: BMP7, bone morphogenetic protein 7; HOTAIR, HoxA transcript antisense RNA; HOTTIP, HoxA transcript at the distal tip; OCT4, octamer-binding protein 4.

[43], cartilage and bone repair [44], programmed cell death [45], and various cancers including gastric cancer [43, 46]. Our knockdown experiments also supported an essential role of BMP7 in promoting cell proliferation, migration, invasion, and colony formation in CS12 cells (Fig. 4E–4H). Moreover, we found that forced expression of BMP7 in CS12iPSLCs, whose BMP7 level was low, increased oncogenic phenotypes such as xenograft tumor formation in SCID mice, invasive and migratory activity, colony formation and cell proliferation (Supporting Information Fig. S5). These results indicate that, at least in gastric cancer, BMP7 behaves as an oncogene.

Our results demonstrated the importance of the HOTTIP/HOTAIR–BMP7 axis in gastric cancer (Fig. 4E–4H). In particular, the increase of tumorigenicity in CS12iPSLCs by HOTAIR knockdown suggests that HOTAIR is a tumor suppressor gene as previously reported in glioblastoma and pediatric ependymoma [47, 48]. However, some studies suggest that HOTAIR is more likely to be an oncogene [42, 49, 50]. Thus, the precise role of HOTAIR may be context-dependent.

The differential recruitment of HOXA13 at positive and negative regulatory sites of the *BMP7* promoter is a new finding, which demonstrates that HOXA13 can play either a positive or a negative role in expression of the same gene. Most previous studies only show the oncogenic role of HOXA13. Our study reveals that HOXA13 has an anti-oncogenic activity in CS12iPSLCs possibly through suppressing BMP7 expression (Figs. 3F, 3H, 3J, 6C, 7D). This study also demonstrates a novel, opposing regulation of the BMP7 expression pattern, which is regulated by HOTTIP- and HOTAIR-mediated epigenetic changes at the S1 and S2 sites of *BMP7* promoter, respectively (Fig. 7). These epigenetic changes are differentially regulated in CS12 and CS12iPSLCs, which represent different gastric cancer stages. Thus, the present study reveals the complexity of epigenetic regulation of BMP7 expression during the development of gastric cancer.

This study has identified the differential effects of HOTTIP and HOTAIR on the S1 and S2 sites of *BMP7* promoter that is correlated with upregulated and downregulated BMP7 expression, respectively. However, this finding does not fully explain the differential HOXA13 binding of S1 and S2 sites that is also correlated with BMP7 expression. Several issues need further investigation. First, the recruitment of HOXA13 at the S1 and S2 sites after knockdown of HOTTIP and HOTAIR can be examined to show the effect of lncRNAs on HOXA13 recruitment to the *BMP7* promoter. Second, whether HOTTIP and HOTAIR directly target to S1 and S2 sites, respectively, or HOTTIP and HOTAIR regulate epigenetic changes at S1 and S2 sites indirectly is still unclear. Although our data showed the increased recruitment of WDR5/MLL to the HOTTIP-regulated S1 site and EZH2/JARID2 to the HOTAIR-regulated S2 site (Fig. 5), we did not yet check the presence of HOTTIP and HOTAIR at these sites. Third, if HOTTIP and HOTAIR are recruited to the S1 and S2 sites, is HOXA13 involved in this recruitment? Moreover, is HOXA13 required for HOTTIP and HOTAIR recruitment? The interactions between HOXA13 and HOTTIP–HOTAIR, either directly or through other factors such as WDR5 and EZH2/SUZ12, remain to be examined, although they are associated each other (Fig. 5C). We are exploring these questions to elucidate more comprehensively the mechanism underlying BMP7 expression regulated by HOXA13–HOTTIP–HOTAIR in different settings.

## Conclusion

Here, we have identified BMP7 as the key target of HOXA13 to control cell growth, invasion, and migration of human gastric cancer cells. In addition to BMP7, the finding of involvement of the histone methyltransferase (HMT) MLL and EZH2 in regulating BMP7 expression has revealed potential targets for cancer therapy. Several HMT inhibitors are under development to inhibit MLL and EZH2-SUZ12 for therapeutic purpose. Thus, the MLL–WDR5–HOTTIP–HOXA13 axis in CS12 cells can be used to test the therapeutic efficacy of HMT inhibitors. Furthermore, the EZH2–JARID2–HOTAIR–HOXA13 axis in CS12iPSLCs provides a platform to screen carcinogens that increase BMP7 expression.

## Acknowledgments

We thank H. C. Huang and H. Y. Tseng for RNA sequencing work, and K. Itakura for supplying materials and discussion. This work was supported by grants from the Ministry of Science and Technology, Taiwan (MOST-104–2320-B-037–033-MY2; MOST-104–2314-B-037–002; MOST-104–2314-B-037–043); the National Health Research Institutes (NHRI-EX106–10416SI); and Kaohsiung Medical University (KMU-TP105G01, KMU-TP105E21, KMU-DT106006).

## Author Contributions

D.C.W, S.S.W.W, C.J.L., K.W., S. S., C.S.L., and K.K.Y.: conception and design, collection and/or assembly of data, data analysis and interpretation, financial support, manuscript writing, final approval of manuscript; D.C.W., K.W., M.H.T., C.C.K., W.H.L., S.W.W., S.K., M.N., K.K., C.C.Y., Y.T.C., C.Y.C., and K.K.Y.: collection and/or assembly of data, administrative support; Y.L.L., Y.C.L., S.K., K.K., M.N., K.K.K., Y.H.Y., H.M., Y.N., C.S.S.L., S.S., K. N., and K.K.Y.: data analysis and interpretation; D.C.W., K.W., C.S.L., and K.K.Y.: manuscript writing; H.M., Y.N., K.N.,and S.S.: provision of study material.

## Disclosure of Potential Conflicts of Interest

The authors indicated no potential conflicts of interest.

## References

1 Krumlauf R. Hox genes in vertibrate development. Cell 1994;28:191–201.

2 Huang T, Chesnokov V, Yokoyama KK et al. Expression of the HOXA13 gene correlates to hepatitis B and C virus associated HCC. Biochem Biophys Res Commun 2001; 281:1041–1044.

3 Gu ZD, Shen LY, Wang H et al. HOXA13 promotes cancer cell growth and predicts poor survival of patients with esophageal squamous cell carcinoma. Cancer Res 2009; 69:4969–4973.

4 Cillo C, Schiavo G, Cantile M et al. The HOX gene network in hepatocellular carcinoma. Int J Cancer 2011;129:2577–2587.

5 Shah N, Sukumar S. The Hox genes and their roles in oncogenesis. Nat Rev Cancer 2010;10:361–371.

**6** Han Y, Tu WW, Wen YG et al. Identification and validation that up-expression of HOXA13 is a novel independent prognostic marker of a worse outcome in gastric cancer based on immunohistochemistry. Med Oncol 2013;30:564.
**7** Wang SS, Wuputra K, Liu CJ et al. Oncogenic function of the homeobox A13-long noncoding RNA HOTTIP-insulin growth factor-binding protein 3 axis in human gastric cancer. Oncotarget 2016;7:36049–36064.
**8** Morgan EA, Nguyen SB, Scott V et al. Loss of Bmp7 and Fgf8 signaling in Hoxa13-mutant mice causes hypospadia. Development 2003; 130:3095–3109.
**9** Knosp WM, Scott V, Bachinger HP et al. HOXA13 regulates the expression of bone morphogenetic proteins 2 and 7 to control distal limb morphogenesis. Development 2004;131:4581–4592.
**10** Alarmo EL, Pärssinen J, Ketolainen JM et al. BMP7 influences proliferation, migration, and invasion of breast cancer cells. Cancer Lett 2009;275:35–43.
**11** Buijis JT, Rentsch CA, van der Horst G et al. BMP7, a putative regulator of epithelial homeostasis in the human prostate, is a potent inhibitor of prostate cancer bone metastasis in vivo. Am J Pathol 2007;171: 1047–1057.
**12** Grgurevic L, Christensen GL, Schulz TJ et al. Bone morphogenetic proteins in inflammation, glucose homeostasis and adipose tissue energy metabolism. Cytokine Growth Factor Rev 2016;27:105–118.
**13** Wang KC, Yang YW, Liu B et al. A long noncoding RNA maintains active chromatin to coordinate homeotic gene expression. Nature 2011;472:120–124.
**14** Yang YW, Flynn RA, Chen Y et al. Essential role of lncRNA binding for WDR5 maintenance of active chromatin and embryonic stem cell pluripotency. Elife 2014;3:e02046.
**15** Quagliata L, Matter MS, Piscuoglio S et al. Long noncoding RNA HOTTIP/HOXA13 expression is associated with disease progression and predicts outcome in hepatocellular carcinoma patients. Hepatology 2014;59:911–923.
**16** Zhang H, Zhao L, Wang YX et al. Long non-coding RNA HOTTIP is correlated with progression and prognosis in tongue squamous cell carcinoma. Tumour Biol 2015;36: 8805–8809.
**17** Li Z, Zhao X, Zhou Y et al. The long noncoding RNA HOTTIP promotes progression and gemcitabine resistance by regulating HOXA13 in pancreatic cancer. J Transl Med 2015;13:84.
**18** Rinn JL, Kertesz M, Wang JK et al. Functional demarcation of active and silent chromatin domains in human HOX loci by noncoding RNAs. Cell 2007;129:1311–1323.
**19** Miao Z, Ding J, Chen B et al. HOTAIR overexpression correlated with worse survival in patients with solid tumors. Minerva Med 2016;107:392–400.
**20** Wang Y, Dang Y, Liu J et al. The function of homeobox genes and lncRNAs in cancer. Oncol Lett 2016;12:1635–1641.
**21** Pan J, Nakade K, Hunag YC et al. Suppression of cell-cycle progression by Jun dimarization protein-2 (JDP2) involves down-regulation of cycling A2. Oncogene 2010;29: 6245–6256.
**22** Chiou SS, Wang SS, Wu DC et al. Control of oxidative stress and generation of induced pluripotent stem cell-like cells by Jun Dimerization Protein 2. Cancers (Basel) 2013;5: 959–984.
**23** Liu J, Han Q, Peng T et al. The oncogene c-Jun impedes somatic cell reprogramming. Nat Cell Biol 2015;17:856–867.
**24** Takahashi K, Yamanaka S. Induction of pluripotent stem cells from mouse embryonic and adult fibroblast cultures by defined factors. Cell 2006;126:663–676.
**25** Ramos-Mejia V, Fraga MF, Menendez P. iPSCs from cancer cells: Challenges and opportunities. Trends Mol Med 2012;18:245–247.
**26** Semi K, Matsuda Y, Ohnishi K et al. Cellular reprogramming and cancer development. Int J Cancer 2013;132:1240–1248.
**27** Yang YC, Wang SW, Hung HY et al. Isolation and characterization of human gastric cell lines with stem cell phenotypes. J Gastroenterol Hepatol 2007;22:1460–1468.
**28** Miyoshi H, Takahashi M, Gage FH et al. Stable and efficient gene transfer into the retina using an HIV-based lentiviral vector. Proc Natl Acad Sci USA 1997;94:10319–10323.
**29** Kuo KK, Lee KT, Chen KK et al. Positive feedback loop of OCT4 and c-JUN expedites cancer stemness in liver cancer. Stem Cells 2016;34:2613–2624.
**30** Saito S, Sawai K, Minamihashi A et al. Derivation, maintanance and induction of the differentiation in vitro of equuine embryonic stem cells. In: Turksen K, ed. Embryonic Stem Cell Protocol. Totowa, NJ: Humana Press, 2005:59–79.
**31** Wang SW, Wang SS, Wu DC et al. Androgen receptor-mediated apoptosis in bovine testicular induced pluripotent stem cells in response to phthalate esters. Cell Death Dis 2013;4:e907.
**32** Nussbaum R, McInnes R, Willard H. Thompson & Thompson, Genetics in Medicine (Eighth ed.). Canada: Elsevier Inc., 2015.
**33** Tanigawa S, Lee CH, Lin CS et al. Jun dimerization protein 2 is a critical component of the Nrf2/MafK complex regulating the response to ROS homeostasis. Cell Death Dis 2013;4:e921.
**34** Kawasaki H, Eckner R, Yao TP et al. Distinct roles of the co-activators p300 and CBP in retinoic-acid-induced F9-cell differebntiation. Nature 1998;393:284–289.
**35** Kawasaki H, Song J, Eckner R et al. p300 and ATF-2 are components of the DRF complex, which regulates retinoic acid- and E1A-mediated transcription of the c-jun gene in F9 cells. Genes Dev 1998;12:233–245.
**36** Jain R, Devine T, George AD et al. RIP-ChiP analysis: RNA-Binding protein immunoprecipitation-microarray (Chip) profiling. Methods Mol Biol 2011;703:247–263.
**37** Yang YC, Wang SW, Wu IC et al. A tumorigenic homeobox (HOX) gene expressing human gastric cell line derived from putative gastric stem cell. Eur J Gastroenterol Hepatol 2009;21:1016–1023.
**38** McCabe CD, Innis JW. A genomic approach to the identification and characterization of HOXA13 functional binding elements. Nucleic Acids Res 2005;33:6782–6794.
**39** Williams TM, Williams ME, Kuick R et al. Candidate downstream regulated genes of HOX group 13 transcription factors with and without monomeric DNA binding capability. Dev Biol 2005;279:462–480.
**40** Kawai S, Sugiura T. Characterization of human bone morphogenetic protein (BMP)-4 and −7 gene promoters: Activation of BMP promoters by Gli, a sonic hedgehog mediator. Bone 2001;29:54–61.
**41** Sanulli S, Justin N, Teissandier A et al. Jarid2 methylation via the PRC2 complex regulates H3K27me3 deposition during cell differentiation. Mol Cell 2015;57:769–783.
**42** Bhan A, Mandal SS. LncRNA HOTAIR: A master regulator of chromatin dynamics and cancer. Biochim Biophys Acta 2015;1856:151–164.
**43** Boon MR, van der Horst G, van der Pluijm G et al. Bone morphogenetic protein 7: A broad-spectrum growth factor with multiple target therapeutic potency. Cytokine Growth Factor Rev 2011;22:221–229.
**44** Salazar VS, Gamer LW, Rosen V. BMP signalling in skeletal development, disease and repair. Nat Rev Endocrinol 2016;12:203–221.
**45** Kaltcheva MM, Anderson MJ, Harfe BD et al. BMPs are direct triggers of interdigital programmed cell death. Dev Biol 2016;411: 266–276.
**46** Aoki M, Ishigami S, Uenosono Y et al. Expression of BMP-7 in human gastric cancer and its clinical significance. Br J Cancer 2011; 104:714–718.
**47** Balci T, Yilmaz Susluer S, Kayabasi C et al. Analysis of dysregulated long non-coding RNA expressions in glioblastoma cells. Gene 2016;590:120–122.
**48** Chakravadhanula M, Ozols VV, Hampton CN et al. Expression of the HOX genes and HOTAIR in atypical teratoid rhabdoid tumors and other pediatric brain tumors. Cancer Genet 2014;207:425–428.
**49** Gupta RA, Shah N, Wang KC et al. Long non-coding RNA HOTAIR reprograms chromatin state to promote cancer metastasis. Nature 2010;464:1071–1076.
**50** Hajjari M, Salavaty A. HOTAIR: An oncogenic long non-coding RNA in different cancers. Cancer Biol Med 2015;12:1–9.


See www.StemCells.com for supporting information available online.